


RESEARCH

Open Access



# scRNA-seq reveals that VEGF signaling mediates the response to neoadjuvant anlotinib combined with PD-1 blockade therapy in non-small cell lung cancer

Ziqi Huang<sup>1†</sup>, Li Li<sup>1†</sup>, Xiaohe Zhao<sup>1†</sup>, Haixia Jin<sup>1</sup>, Meng Shen<sup>1</sup>, Baihui Li<sup>2</sup>, Yu Zeng<sup>1</sup>, Qinfen Zhang<sup>1</sup>, Qiyu Wang<sup>1</sup>, Meng Wang<sup>3\*</sup> and Lili Yang<sup>1\*</sup> 

## Abstract

**Background** Clinical trials have shown that neoadjuvant anlotinib combined with PD-1 blockade therapy can prolong the survival of patients with driver gene negative non-small cell lung cancer (NSCLC), but some patients fail to benefit from the combination therapy.

**Methods** To explore the potential drug resistance mechanism and predict the efficacy of neoadjuvant therapy in NSCLC patients, we used scRNA-seq to observe and analyze the dynamic changes of immune cells, stromal cells and cancer cells in NSCLC patients who received neoadjuvant combination therapy. We analyzed transcriptome data of ~47,000 single cells from 9 NSCLC patients, including 3 treatment naïve patients, 3 post-treatment patients with major pathological response (MPR), and 3 Non-MPR patients. Subsequently, the infiltration of immune cells was detected by immunohistochemistry and multiplex immunofluorescence in NSCLC.

**Results** In MPR patients, we found that neoadjuvant therapy reduced the expression of the T cell exhausted signature, reduced the transition of T<sub>H</sub>17 cells to Tregs, and enhanced the positive feedback between CD4<sup>+</sup> T cells and PAX5<sup>+</sup> memory B cells. In Non-MPR patients, tumor-associated macrophages (TAMs) dampen therapeutic efficiency by being the hub of cell communication. TAMs and fibroblasts stimulate endothelial cells via VEGF, endothelial ZEB1 may up-regulate FLT1 (VEGFR) expression in response to anlotinib, and VEGFR<sup>+</sup> endothelial cell signature can predict survival of NSCLC cohort in TCGA. In addition, PLA2G4A, the key enzyme in the VEGF pathway, was highly expressed in the tumor cells of Non-MPR patients after anlotinib treatment. In 135 NSCLC patients, we confirmed by immunohistochemistry that PLA2G4A was positively correlated with poor prognosis and Tregs infiltration.

**Conclusion** In conclusion, VEGF signaling dependent dynamic changes in endothelial and epithelial cells are deeply involved in the formation of anlotinib resistance and immunosuppression phenotypes in NSCLC patients.

**Keywords** Neoadjuvant immunotherapy, Anlotinib, PD-1 blockade, NSCLC, Tumor microenvironment, Single-cell, VEGFR, PLA2G4A

<sup>†</sup>Ziqi Huang, Li Li and Xiaohe Zhao have contributed equally to this work.

\*Correspondence:

Meng Wang  
wangmeng@tjmuch.com  
Lili Yang  
yanglili@tjmuch.com

Full list of author information is available at the end of the article



© The Author(s) 2025. **Open Access** This article is licensed under a Creative Commons Attribution-NonCommercial-NoDerivatives 4.0 International License, which permits any non-commercial use, sharing, distribution and reproduction in any medium or format, as long as you give appropriate credit to the original author(s) and the source, provide a link to the Creative Commons licence, and indicate if you modified the licensed material. You do not have permission under this licence to share adapted material derived from this article or parts of it. The images or other third party material in this article are included in the article's Creative Commons licence, unless indicated otherwise in a credit line to the material. If material is not included in the article's Creative Commons licence and your intended use is not permitted by statutory regulation or exceeds the permitted use, you will need to obtain permission directly from the copyright holder. To view a copy of this licence, visit <http://creativecommons.org/licenses/by-nc-nd/4.0/>.

## Background

Neoadjuvant immunotherapy can significantly prolong the survival of driver-negative NSCLC patients, but many patients still do not benefit from single agent [1, 2]. Novel clinical trials trying to reshape the immune microenvironment using different neoadjuvant combination therapy strategies, hoping to solve this urgent dilemma [3, 4]. To our delight, clinical trials have shown that immunotherapy combined with anti-angiogenic therapy has achieved better results than single drug therapy in a variety of solid tumors [5, 6]. In mechanism, tumor cells release pro-angiogenic factors such as vascular endothelial growth factor A (VEGFA), which act on vascular endothelial cells to generate blood vessels [7]. Moreover, growth factors such as VEGFA reduce the adhesion and migration of immune cells [8], inhibit the maturation and the differentiation of hematopoietic precursor cells [9], and promote the expression of immune checkpoint ligand in CD8<sup>+</sup> T cell [10]. These results provide strong evidence that the combination of anti-angiogenic therapy and immunotherapy has a solid rationale.

Anlotinib, a multityrosine kinase inhibitor for vascular endothelial growth factor receptor (VEGFR) [11]. Mechanistically, anlotinib may affect the efficacy by regulating the expression of PD-L1 in micro-conduit endothelium [12, 13]. Moreover, anlotinib could increase the infiltration of CD8<sup>+</sup> T cells by inducing CCL5 and promote the apoptosis of cancer-associated fibroblasts by inhibiting AKT pathway, thereby improving the efficacy of PD-1 blockade [14, 15]. These results suggested the potential synergistic effect of anlotinib combined with immune checkpoint inhibitors [16, 17]. A recent study of second-line anlotinib combined with PD-1 blockade therapy in patients with advanced NSCLC patients showed an objective response rate of 23.9% and a disease control rate of 85.1%, and exploratory analysis highlighted that 17 patients who were intolerant to previous immune-related regimens might have a superior prognosis (median overall survival: 22.3 months vs 12.5 months) [18].

In view of these encouraging results, we conducted a clinical trial of neoadjuvant anlotinib combined with PD-1 blockade therapy in NSCLC. We found that most patients with NSCLC reached the criteria for surgical resection after 4 cycles of combination therapy, and the adverse reactions were significantly less than those of chemotherapy. To explore the mechanism of drug resistance and predict patient response, we performed scRNA-seq to observe and analyze the dynamic changes of immune cells, stromal cells and cancer cells from the NSCLC patients who received neoadjuvant anlotinib

combined with PD-1 blockade therapy and verified in an independent cohort.

## Methods

### Patients information

The inclusion criteria were patients with histologically or cytologically confirmed stage IIB-IIIB (N2) NSCLC (according to the 8th edition of the International Association for the Study of Lung Cancer (IASLC) staging manual for thoracic tumors) had not received surgery, chemotherapy, radiotherapy or biological therapy; the primary tumor or lymph node metastasis was negative for EGFR/ALK/ROS1. The neoadjuvant regimen consisted of 4 cycles of anlotinib (10 mg orally once daily for 2 consecutive weeks, 3 weeks per cycle) combined with camrelizumab (200 mg intravenously on day 1, 3 weeks per cycle). On the basis of the assessment of operability, surgical resection was performed 3–7 weeks after the last dose of anlotinib. Six patients were enrolled in this study from December 2022 to December 2023. In addition, we collected another biopsy samples in 3 pre-treatment patients downloaded from Genome Sequence Archive database, under accession number HRA001033.

### Preparation of single cell isolation

The Isolation Kit furnished by Shanghai Biotechnology Corporation was exploited. Tissue samples were homogenized and transformed into a liquid state with a tissue homogenizer, succeeded by thorough lysis on ice. The resultant tissue lysates were filtrated through a 40 µm cell sieve to eliminate impurities, and the supernatant was meticulously aspirated by means of centrifugation while preserving the precipitate. Nuclear suspensions were obtained in accordance with the standard protocols of the kit. Ultimately, 5 µL of each nuclear suspension was aliquoted and stained with trypan blue for the quantification of cell nuclei and microscopic examination.

### Single-cells RNA sequencing

The Gel Beads-in-emulsion was transferred to a PCR instrument for reverse transcription in Shanghai Biotechnology Corporation, and the cDNA strand with Barcode and UMI information was obtained according to the standard procedure of the system, followed by purification, amplification and detection of concentration. After passing the quality inspection, cluster generation and hybridization of the first sequencing primers were completed, and the flow cell with cluster was carried on the computer.

### Data generation and quality control

Single-cell data were transferred for cell expression matrices using Rhapsody. The distributions of UMI, genes, mitochondria, and ribosomes of each sample were statistically analyzed herein to calculate the filtering threshold required for each sample. Moreover, cells with a red blood cell gene proportion exceeding 1% were filtered out, and if the mitochondrial proportion filtering threshold of a single sample exceeds 25%, it would be filtered again at the 25% threshold. According to the total number of reads expressed by cells and the proportion of mitochondrial genes in reads, the data quality control was performed to filter out most double cells. To eliminate doublets and multiples, the Scrublet method was employed to filter double cells once again. The Scrublet algorithm randomly extracts pairs of barcodes to simulate double cells and adds them to the original expression matrix. According to the clustering results, the cells are scored (doublet score), the higher the score, the more likely they are double cells. Here, 0.2 was selected to cluster all cells (including the simulated double cells).

### Integrated analysis and dimensionality reduction of multiple samples

TOP 2000 variant genes of each sample were first identified for later integration analysis. In this experiment, the Harmony algorithm was used to integrate multiple samples of single cells. Since Harmony uses soft clustering, each single cell can be corrected linearly for the soft cluster assignment by a linear combination of multiple factors, repeating these steps until the cell cluster assignment is stable.

### Determination of major cell classes

The cell types were annotated by combining the single-cell sequencing cell type annotation software SingleR (version v1.0.0) and marker genes. SingleR selects the highly variable genes among different cell types in the reference database, and then calculates the correlation between the predicted cells and the reference database. By continuously eliminating the worst correlation type,

SingleR calculates the correlation, and finally obtains the type annotation of cells.

### CNV identification of malignant cells

To identify malignant cells from epithelia, we used the inferCNV (version 0.1.0) to estimate the copy number variations (CNVs). The myeloid cells were used as normal reference, and the parameters were default.

### Gene function enrichment and gene activity analysis

Based on the sample grouping information, differential expression analysis is performed for each cluster. Genes with  $FC > 1.5$  and  $P < 0.05$  relative to other genes were defined as differentially expressed genes between groups. Then, the functional enrichment in each cluster was analyzed by KEGG and GO, and significant enriched functional pathways were selected to explore the functional heterogeneity between the groups. GSVA was performed using the default parameters to assess the activity of the gene set. Each cluster was compared with other clusters to explore the functional heterogeneity of different cluster cells.

### Cell–cell interaction and trajectory analysis

We used cellchat (version v0.5.0) to infer cellular interactions between different cell types. CellChat leverages scRNA-seq data to infer, visualize, and analyze intercellular communication networks. CellChat models communication probabilities and identifies important communication networks. It is further subdivided into signal transduction pathways by detecting ligand–receptor pairs in the cell. We used the default parameter RNA velocity to determine the potential lineage differentiation of the cells.

### Immunohistochemistry and multiplex immunofluorescence

Tissue samples were processed into tissue microarrays, embedded in paraffin. The microarray underwent immunohistochemical staining following standard procedures. Incubation was conducted using the PLA2G4A monoclonal antibody (Proteintech, 68133-1-Ig), CD68 monoclonal antibody (invitrogen, 14-0688-82), FoxP3

(See figure on next page.)

**Fig. 1** scRNA-seq analysis of neoadjuvant NSCLC samples. **A** Single-cell RNA sequencing was performed using the 10X genomics method for cell sampling and cDNA library preparation. **B** Bubble map of normalized expression of representative cell-lineage marker genes according to the major cells. **C** tSNE (t-distributed stochastic neighbor embedding) plot of all cells, with major cell types color-coded. **D** Bar plot of the proportions of major cell-lineages for each patient. **E** Box plot of fractions of T cells, B cells, myeloid cells in TN (n = 3), MPR (n = 3), and Non-MPR (n = 3) patients. The middle line represents the median, and the lower and upper lines represent the 25th and 75th percentiles, respectively, with each point corresponding to one sample. t test was used for data analysis. **F** Heat map of the main pathway patterns of incoming and outgoing signaling molecules. **G** Shell map of the interactions among cell types

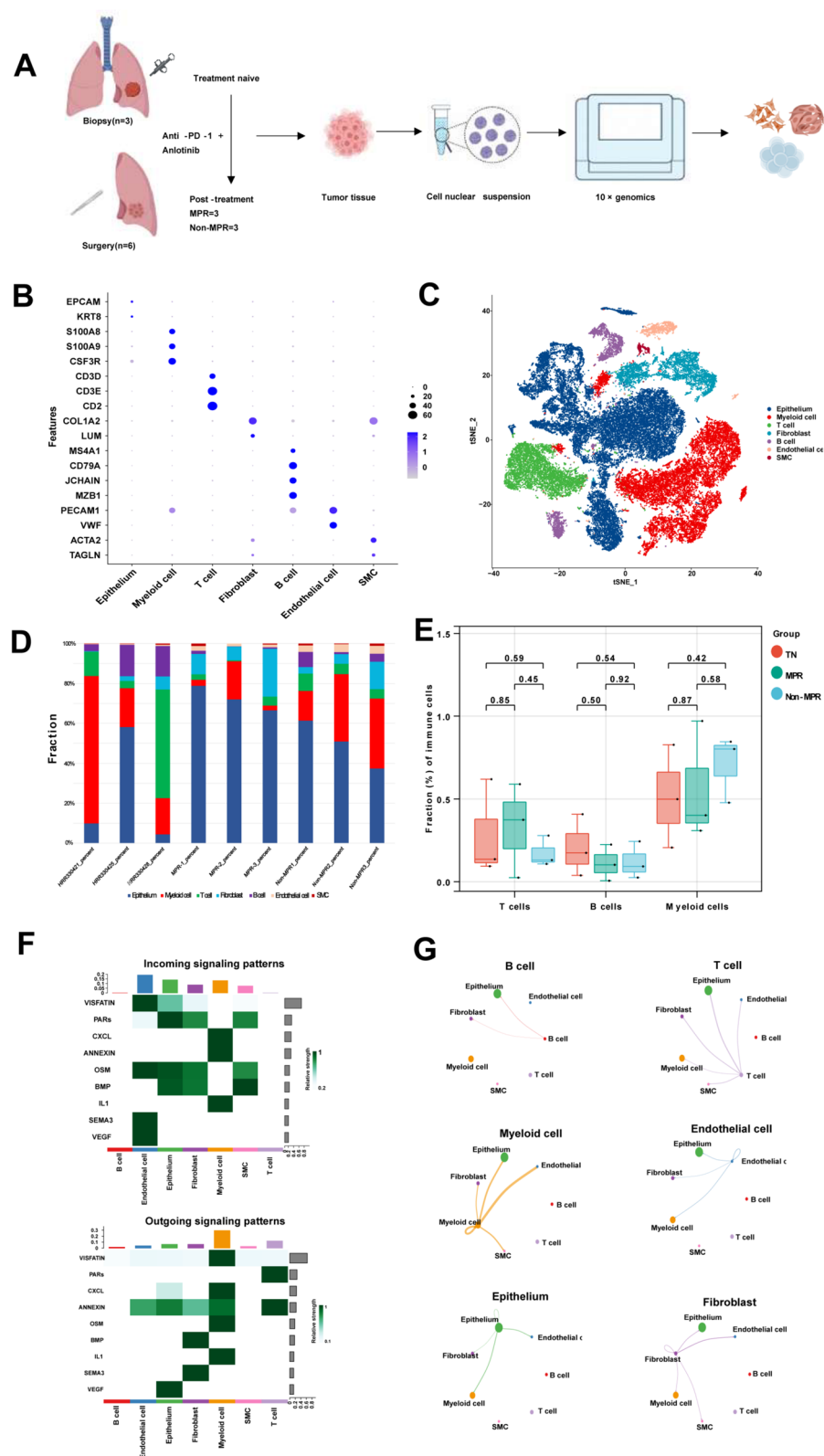


**Fig. 1** (See legend on previous page.)



monoclonal antibody (abcam, ab215206), CD8 monoclonal antibody (abcam, ab245118), CTLA4 monoclonal antibody (abcam, ab237712), CD20 monoclonal antibody (abcam, ab64088), and CD4 monoclonal antibody (abcam, ab133616).

Multiplex immunofluorescence staining was performed according to the manufacturer's protocol (PerkinElmer, Opal<sup>®</sup>Kit) to display cellular markers. Scanning and imaging were performed using a Vectra Polaris Automated Quantitative Pathology Imaging system (PerkinElmer, Massachusetts, USA) at 200× magnification with the same exposure time.

### Cell culture

The cell lines used in this study, including human lung cancer cell line A549, human endothelial cell line HUVEC and human macrophage cell line THP-1, were obtained by ATCC by STR typing and tested to be free of mycoplasma contamination. Cultures were grown in DMEM or RPMI-1640 basal medium supplemented with 10% fetal bovine serum as medium at 37 °C according to the manufacturer's instructions in a humidified atmosphere of 95% air and 5% carbon dioxide.

THP-1 were treated with 5 pg/ml PMA (P61-900D, SinoBiological) in order to stimulate the transformation of macrophages. After 48 h of stimulation, THP-1 derived macrophages were pre-incubated with the supernatant conditioned medium (CM) of A549 cells for 48 h before co-culturing with HUVEC at a 1:1 ratio for 48 h. Anlotinib (20 μM) were added to the mix.

### RT-qPCR

Total RNA was extracted using TRIZOL reagent (Invitrogen, Carlsbad, CA, USA). Reverse transcription was performed according to standard protocols to prepare complementary DNA, using the reverse transcription Kit (Takara, #RR037Q). RT-qPCR analysis was performed on the QuantStudio 5 real-time PCR system (Thermo Electron, USA, #A28575) using 2X SG Fast qPCR Mix (Sangon, #B639271). The primers used are listed in Additional file 2: Table S4.

### Statistical analysis

GraphPad Prism version 9.0 was used for graph drawing and statistical analysis. Kaplan–Meier curves were used and estimated by the log-rank test, and multivariate regression analysis was performed by Cox regression analysis in Sangerbox (<http://www.sangerbox.com/tool>). Wilcoxon test was used to assess differences in immune cell densities; Pearson-correlation was used to assess linear relationships between continuous variables. The following significance levels were used: \* $P < 0.05$ ; \*\* $P < 0.01$ ; \*\*\* $P < 0.001$ ; NS,  $P > 0.5$ .

### Results

#### scRNA-seq analysis of neoadjuvant NSCLC samples

We collected tumor samples from 6 patients with advanced NSCLC who received surgical resections after neoadjuvant combination therapy for analysis by scRNA-seq. According to the results of pathological evaluation, the 6 patients were divided into MPR group ( $n = 3$ ) and Non-MPR ( $n = 3$ ). Moreover, scRNA-seq data from biopsy samples collected as treatment naïve (TN;  $n = 3$ ) were additionally downloaded for subsequent analysis with data from the other 6 patients (Additional file 2: Table S1). Transcriptomes from 47,294 cells were selected for further analysis following quality control and removal of duplications (Fig. 1A).

Unsupervised cluster analysis of all cells from 9 cases identified 23 clusters (Additional file 1: Fig. S1A, B), which were annotated as epithelial cells, endothelial cells, fibroblasts, T cells, B cells, smooth muscle cells and myeloid cells based on the list of marker genes (Fig. 1B, C, Additional file 2: Table S2).

To investigate the remodeling effect of treatment on tumor microenvironment, we listed the proportions of cells in patients (Fig. 1D). In a limited number of cases, we found that the fractions of T cells decreased, and myeloid cells increased in Non-MPR patients after therapy (Fig. 1E). Then we explored the interactions among cell types in NSCLC. Epithelial cells interacted with endothelial cells through VEGF signaling (Fig. 1F), whereas myeloid cells interacted strongly with fibroblasts, endothelial cells, and epithelial cells (Fig. 1G). Based

(See figure on next page.)

**Fig. 2** The transition of T cells to Tregs suggested a poor pathologic response. **A** tSNE plot of T cells color-coded by clusters. **B** Heat map of normalized expression of canonical T/NK cell marker genes among clusters. **C** Box plot of fractions of T cells in TN ( $n = 3$ ), MPR ( $n = 3$ ), and Non-MPR ( $n = 3$ ) patients. The middle line represents the median, the lower and upper lines represent the 25th and 75th percentiles, respectively, with each point corresponding to one sample. t test was used for data analysis. **D** Box plot of the average exhausted signature scores for CD4\_CCR7, CD8\_GZMK, T\_THEMIS and Treg\_CTLA4 in TN ( $n = 3$ ), MPR ( $n = 3$ ), and Non-MPR ( $n = 3$ ) patients. t test was used for data analysis. **E** GSEA analyses the functional heterogeneity of cells in different clusters, showing only the top 10 terms with NES values in each cluster. **F** In situ multiplex immunofluorescence images of FoxP3, CTLA4, and CD4 in MPR and Non-MPR tumor tissues. **G** The developmental trajectory of CD4<sup>+</sup> T cells inferred by Monocle2. The T\_THEMIS was the roots of differentiation, and the naïve T CD4\_CCR7 and the Treg\_CTLA4 were in the end-point state. **H** Heat map of the interactions between cancer cells and T\_THEMIS cells



on the distribution of various types of cells (Additional file 1: Fig. S1C), we analyzed the critical contribution of subpopulation markers to the microenvironment and their impact on the prognosis.

### The transition of T cells to Tregs suggested a poor pathologic response

First, we re-clustered T/NK cells and identified 7 clusters (Fig. 2A, B). These includes 1 subtype of T cells (T\_THEMIS; Additional file 1: Fig. S2A), 1 subtype of NK cells (NK\_KLRD1), 1 subtype of CD8<sup>+</sup> T cells (CD8\_GZMK), 3 subtypes of CD4<sup>+</sup> T cells (CD4\_CCR7, CD4\_CD40LG, and CD4\_CD28), and 1 subtype of Treg cells (Treg\_CTLA4).

Then, we compared fractions and found that CD4<sup>+</sup> T cells were much more than CD8<sup>+</sup> T cells (Additional file 1: Fig. S2B). Relative to TN and Non-MPR, Treg\_CTLA4 cells (highly expressed IL2RA and TIGIT) decreased, and CD4\_CCR7 cells increased in MPR patients (Fig. 2C). Furthermore, we identified 7 genes (AG3, TIGIT, PCCD1, HAVCR2, CTLA4, LAYN, and ENTPD1) as the exhausted signature of T cell. The exhausted signatures of CD4\_CCR7 cells were significantly decreased after therapy, especially in MPR patients (Fig. 2D, Additional file 1: Fig. S2C). In addition, exhausted signature of Tregs were lower in MPR compared with Non-MPR patients (Fig. 2D). We found that Treg\_CTLA4 had a vigorous pyruvate metabolism, whereas CD4\_CCR7 and CD4\_CD40LG were dominated by oxidative phosphorylation (Fig. 2E). Consistently, multiplex immunofluorescence (mIHC) showed that CTLA4<sup>+</sup>FoxP3<sup>+</sup>CD4<sup>+</sup> T cell were much more in Non-MPR compared with MPR patients (Fig. 2F), indicating a decrease of Treg cells in MPR patients after treatment.

Meanwhile, T\_THEMIS cells increased after combination therapy (Fig. 2C). THEMIS, a canonical regulatory protein involved in the regulation of T cell activation, is a key requirement in the process of positive selection of T cells [19]. We observed more vigorous amino acid metabolism in T\_THEMIS compared to other clusters, such as “Aminoacyl-tRNA biosynthesis” pathway and “Valine, leucine and isoleucine degradation” pathway (Fig. 2E). Therefore, we performed trajectory

analysis to explore the transition of T\_THEMIS cells in tumor tissue (Fig. 2G, Additional file 1: Fig. S2D). There are two transition paths from origin (T\_THEMIS) to naïve T (CD4\_CCR7) and activated Tregs (Treg\_CTLA4). The analysis showed that differentiation of T\_THEMIS cells is critical for the expansion of Tregs. We found that the distribution of T\_THEMIS cell in pseudo-time can be divided into two states (Additional file 1: Fig. S2E). T\_THEMIS cell highly expressed DLG2 in primary state, while the expression of MHC-II genes (HLA-A and HLA-C) was upregulated in the activated state. CellPhoneDB analysis revealed that integrins mediate communication between cancer cells and T\_THEMIS cells (Fig. 2H). The mechanism of T\_THEMIS cells transition in the microenvironment after treatment needs to be further explored.

### The positive feedback between PAX5<sup>+</sup> memory B cells and CD4<sup>+</sup> T cells enhanced anti-tumor immunity

We re-clustered B cells into 4 clusters (Fig. 3A), including 3 subtypes of plasma B cells (B1\_PIM2, B2\_JCHAIN and B3\_IGHG3), and 1 memory B cells subtype (B4\_PAX5). Then we compared fractions and found that treatment produced a decrease in plasma B cells and an increase in B4\_PAX5 memory B cells, especially in MPR patients (Fig. 3B). B4\_PAX5 cells highly expressed immunoglobulin receptor (FCRL1), B cell functional regulator (BANK1; Additional file 1: Fig. S3). We found that B4\_PAX5 was enriched in “Fc gamma R-mediated phagocytosis” pathway, “IgA production” pathway, and “B cell receptor signaling” pathway (Fig. 3C).

Moreover, mIHC revealed that CD20<sup>+</sup> cells were more infiltrated in MPR than Non-MPR patients (Fig. 3D). We investigated whether the B4\_PAX5 cells could serve as a predictor of survival. In KMplot, we input PAX5, FCRL1, and BANK1 for multiple gene survival analysis and found that a lower B4\_PAX5 signature was associated with poor prognosis (Fig. 3E). These results suggested that the signature of B4\_PAX5 cell could be used as a prognosis predictor in NSCLC.

We performed CellPhoneDB analysis to investigate the pathways by which T cells communicate with B4\_PAX5

(See figure on next page.)

**Fig. 3** The positive feedback between PAX5<sup>+</sup> memory B cells and CD4<sup>+</sup> T cells enhanced anti-tumor immunity. **A** tSNE plot of B cells color-coded by clusters. **B** Box plot of fractions of B cells in TN (n = 3), MPR (n = 3), and Non-MPR (n = 3) patients. The middle line represents the median, the lower and upper lines represent the 25th and 75th percentiles, respectively, with each point corresponding to one sample. t test was used for data analysis. **C** GSEA analyses the functional heterogeneity of cells in different clusters, showing only the top 10 terms with NES values in each cluster. **D** In situ multiplex immunofluorescence images of B cells in MPR and Non-MPR tumor tissues. **E** Kaplan–Meier plots of overall survival predicted by signatures of B4\_PAX5 memory B cells in NSCLC from TCGA database. **F** Heat map of the interactions between B4\_PAX5 memory B cells and T cells

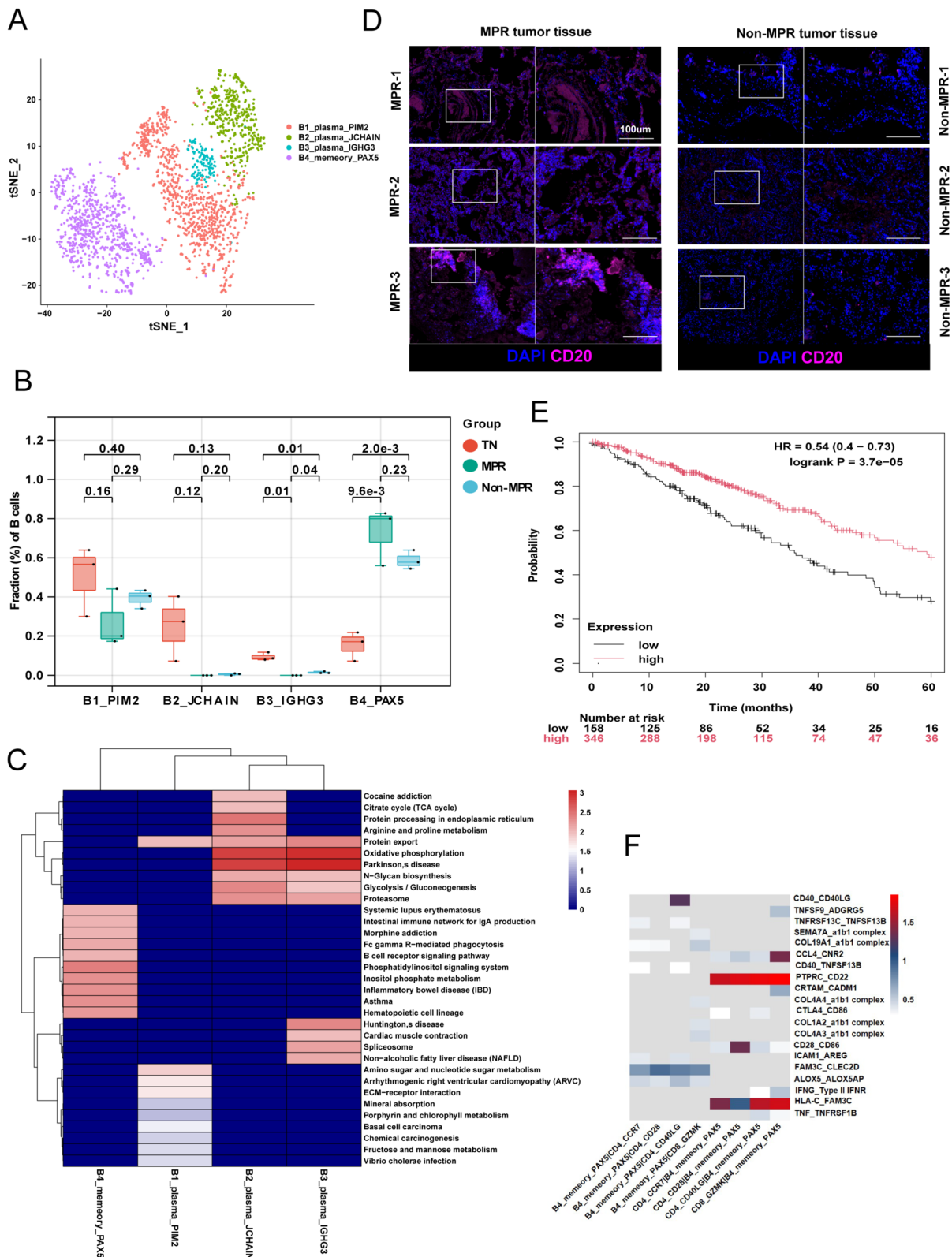


**Fig. 3** (See legend on previous page.)



cells, revealing that B4\_PAX5 cell could interact with T cell through: CCL4-CNR2, IFNG-IFNR (Fig. 3F). The data suggested that in the immune microenvironment, B4\_PAX5 cells are driven by CD40LG from CD4\_CD40LG cells and CD28 from CD4\_CD28 cells, and T cells are activated by FAM3C from B4\_PAX5 cells to strengthen anti-tumor immunity.

#### Tumor-associated macrophages dampen therapeutic efficiency by being the hub of cell communication

The myeloid component was divided into 7 clusters, including 2 subsets of neutrophils, 2 subsets of macrophages, 1 subset of monocytes, 1 subset of DCs, and 1 subset of masts (Fig. 4A, Additional file 1: Fig. S4A). Mac1\_PPARG cells highly expressed M2 marker (MRC1) and the canonical alveolar macrophages markers (FABP4 and MARCO). Mac2\_CD163L1 highly expressed HS3ST2 and LGMN, had a stronger immunosuppressive signature (C1QA, C1QB and APOE; Fig. 4B, C). Indeed, both Mac1\_PPARG and Mac2\_CD163L1 macrophages increased after treatment, and Mac2\_CD163L1 macrophages significantly increased in Non-MPR patients (Fig. 4D). Moreover, mIHC revealed that CD68<sup>+</sup> cells were more infiltrated in Non-MPR than MPR patients (Fig. 4E).

Neutrophil was divided into 2 subsets, including 1 mature subset (CXCR2<sup>high</sup>CXCR4<sup>low</sup>; Neu1\_KCNJ15), and 1 aged subset (CXCR2<sup>low</sup>CXCR4<sup>high</sup>; Neu2\_CXCL10; Fig. 4A, B). Mature Neu1\_KCNJ15 neutrophil highly expressed granules marker (S100A8 and S100A9) and nets marker (LCP1), which after release play a key role in the inflammatory pathway. In the aged subset, Neu2\_CXCL10 cells overexpressed multiple factors, including CXCL9, CXCL10, and VEGFA. Mature Neu1\_KCNJ15 neutrophils decreased after treatment (Fig. 4D). Mon\_VCAN highly expressed monocyte markers (FCN1 and VCAN), and higher MHC-II molecules (HLA-DRA, HLA-DPA1 and CD74), representing mature status. In addition, Mon\_VCAN highly expressed TGFB1, reflecting an immunosuppressive phenotype (Fig. 4B).

Furthermore, cell-to-cell interactions analysis between Mac2\_CD163L1 macrophages and other cells were processed based on the shell map to explore the remodeling effect of treatment on macrophages

(Fig. 1G). The CXCL8, CCL3 and IL18 secreted by Mac2\_CD163L1 macrophages interacted with neutrophils through CXCR1, CCR3 and IL18R. In addition, Mac2\_CD163L1 macrophages were predicted to suppress T\_THEMIS and cancer cells by SPP1 and CXCL2, and fibroblasts communicated with macrophages through integrins (Fig. 4F). These indicate that Mac2\_CD163L1 macrophages suppress the function of T\_THEMIS cells and neutrophils and that cancer-associated fibroblasts are tightly linked to macrophages. And we found that anlotinib treatment significantly enhanced CXCL2/DPP4 signaling between macrophages and tumor cells in co-culture system, while CCL3L3 expression was not significantly changed (Additional file 1: Fig. S4B). Moreover, EGFR and FGFR2 signaling pathways play important roles in the interaction between DC and cancer cells (Additional file 1: Fig. S4C).

#### Endothelial cells may regulate FLT1 in response to anlotinib through ZEB1

The stromal component was divided into 8 subsets, including 2 subsets of endothelial cells, 5 subsets of fibroblasts, and 1 subset of smooth muscle cells (Fig. 5A, Additional file 1: Fig. S5A). Endothelial cells are important targets of anlotinib, we compared the fractions to explore the remodeling effect of combined treatment on endothelial cells. Endo1\_FLT1 cells were blood endothelial cells with the expression of FLT1 (VEGFR), EGFL7 and PECAM1, which enriched in Non-MPR patients (Fig. 5B, C). At the same time, the total fraction of Endo2\_CD36 endothelial cells was close to 5%, which was much less than VEGFR<sup>+</sup> (Endo1\_FLT1) cells. These results suggested that VEGFR expression in endothelial cells of Non-MPR patients is closely related to anlotinib resistance.

Next, we focused on the differences in endothelial transcriptomes after treatment. GSVA analysis showed that amino acid metabolism was the top enriched pathway in MPR endothelial cells, and Non-MPR endothelial cells have significantly primary immunodeficiency (Fig. 5D). Endothelial cells are the main interface between peripheral immune cells and cancer cells and play an important role in transmitting immune signals and presenting epitopes. This suggested

(See figure on next page.)

**Fig. 4** Tumor-associated macrophages dampen therapeutic efficiency by being the hub of cell communication. **A** tSNE plot of myeloid cells color-coded by clusters. **B** Bubble map of normalized expression of canonical myeloid cell marker genes among clusters. **C** tSNE plot of Mac2\_CD163L1 cells marker genes. **D** Box plot of fractions of myeloid cells in TN (n = 3), MPR (n = 3), and Non-MPR (n = 3) patients. The middle line represents the median, the lower and upper lines represent the 25th and 75th percentiles, respectively, with each point corresponding to one sample. t test was used for data analysis. **E** In situ multiplex immunofluorescence images of macrophages in MPR and Non-MPR tumor tissues. **F** Heat map of the interactions among Mac2\_CD163L1 cells, fibroblasts, T\_THEMIS cells and cancer cells

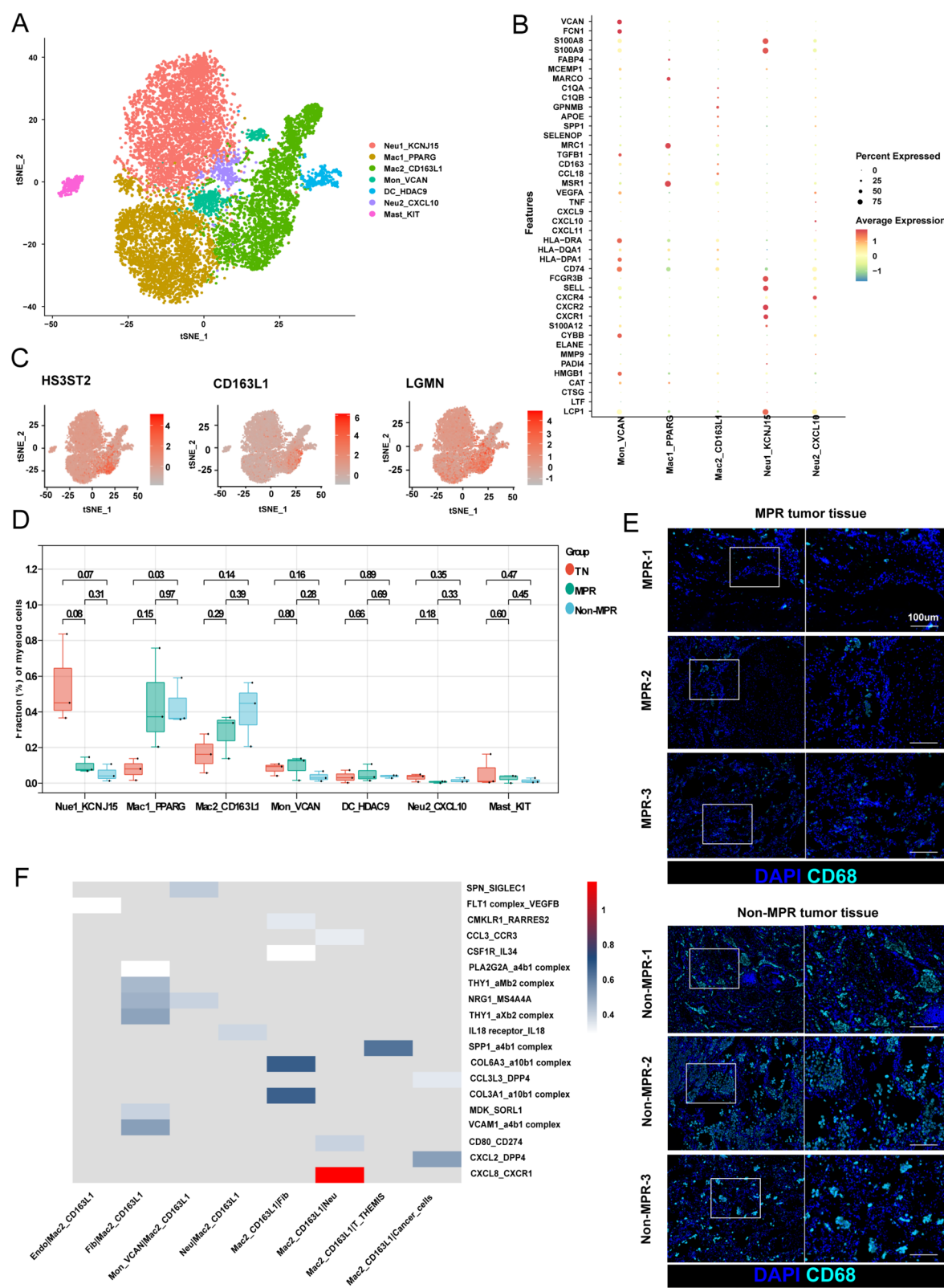


**Fig. 4** (See legend on previous page.)

that Non-MPR endothelial cells are remodeled to downregulate their antigen presentation capacity and immune cell homing activity, thereby promoting a tumor immunoevasive phenotype, and the response to combination therapy may depend on the normalization of endothelial cells.

Finally, we used SCENIC to evaluate the differentially expressed transcription factors and their potential target genes between MPR and Non-MPR endothelial cells (Fig. 5E). ZEB1 was identified as a candidate transcription factor highly expressed in Non-MPR endothelial cells (Fig. 5F). Interestingly, ZEB1 was associated with increased immunosuppressive cell types in the immune microenvironment, and regulator gene of VEGFR show putative ZEB1 binding sites [20], indicating ZEB1 to underline the enhanced immunosuppressive phenotype and regulation of VEGFR in endothelial cell. Moreover, we found that endothelial cells are stimulated by VEGF derived from fibroblasts and Mac2\_CD163L1 (Figs. 4F, 5G) demonstrating the presence of an immunosuppressive cell communication feedback loop in the microenvironment. The co-culture system of macrophages, endothelial cells and tumor cells was employed to verify the effect of anlotinib on cell communication. We found that anlotinib increased the expression of VEGFB but not VEGFA in macrophages and upregulated the expression of VEGFR (FLT1) and ZEB1 in endothelial cells in co-culture system (Additional file 1: Fig. S5B).

#### cPLA2 promoted Tregs infiltration and drug resistance

We used InferCNV analysis to separate malignant and normal cells from 7 subsets of epithelial cells (Fig. 6A, Additional file 1: Fig. S6A). Besides a part of E1\_ABCA3 and E3\_TP63, clusters E4\_ACSL4 and E5\_BCAT1 were inferred to be cancer cell (Additional file 1: Fig. S6B). The fractions of E4\_ACSL4, and E5\_BCAT1 were increased in Non-MPR patients after therapy.

We performed enrichment analysis and noticed that enzymes (PLA2G4A, PLA2G12A and PTK2) in the VEGF signaling pathway were highly expressed in Non-MPR patients compared with TN and MPR (Fig. 6B, C). We speculate that tumor cells upregulate

PLA2G4A (cPLA2) in response to the inhibition of VEGF pathway by anlotinib treatment. We validated the expression changes of VEGF signaling molecules in co-culture system and found that PTK2, PLA2G4A and PLA2G12A were up-regulated in the tumor cells after co-culture with macrophages, and this effect was enhanced by anlotinib treatment (Additional file 1: Fig. S6C). The PLA2 family catalyzes the hydrolysis of membrane phospholipids to release arachidonic acid, which is subsequently metabolized into eicosanoids that mediate inflammatory responses and polarization of macrophages [21]. We analyzed the role of cPLA2 in the immune microenvironment and found that the expression of cPLA2 positively associated with FoxP3 and negatively associated with CD4 (Fig. 6D, E). In addition, cPLA2 was associated with poor prognosis in TCGA (Additional file 1: Fig. S6D), and consistent results were found in our own NSCLC cohort, where PLA2G4A was an independent prognostic factor (Fig. 6F, G, Additional file 2: Table S3). These results suggested that the contribution of PLA2 represented by PLA2G4A to immunosuppression may be dependent on Tregs infiltration, and we speculate that products of arachidonic acid may be involved in the transition of T<sub>H</sub>17 cells to Tregs through SPP1 signaling of TAMs (Fig. 4F).

#### Discussion

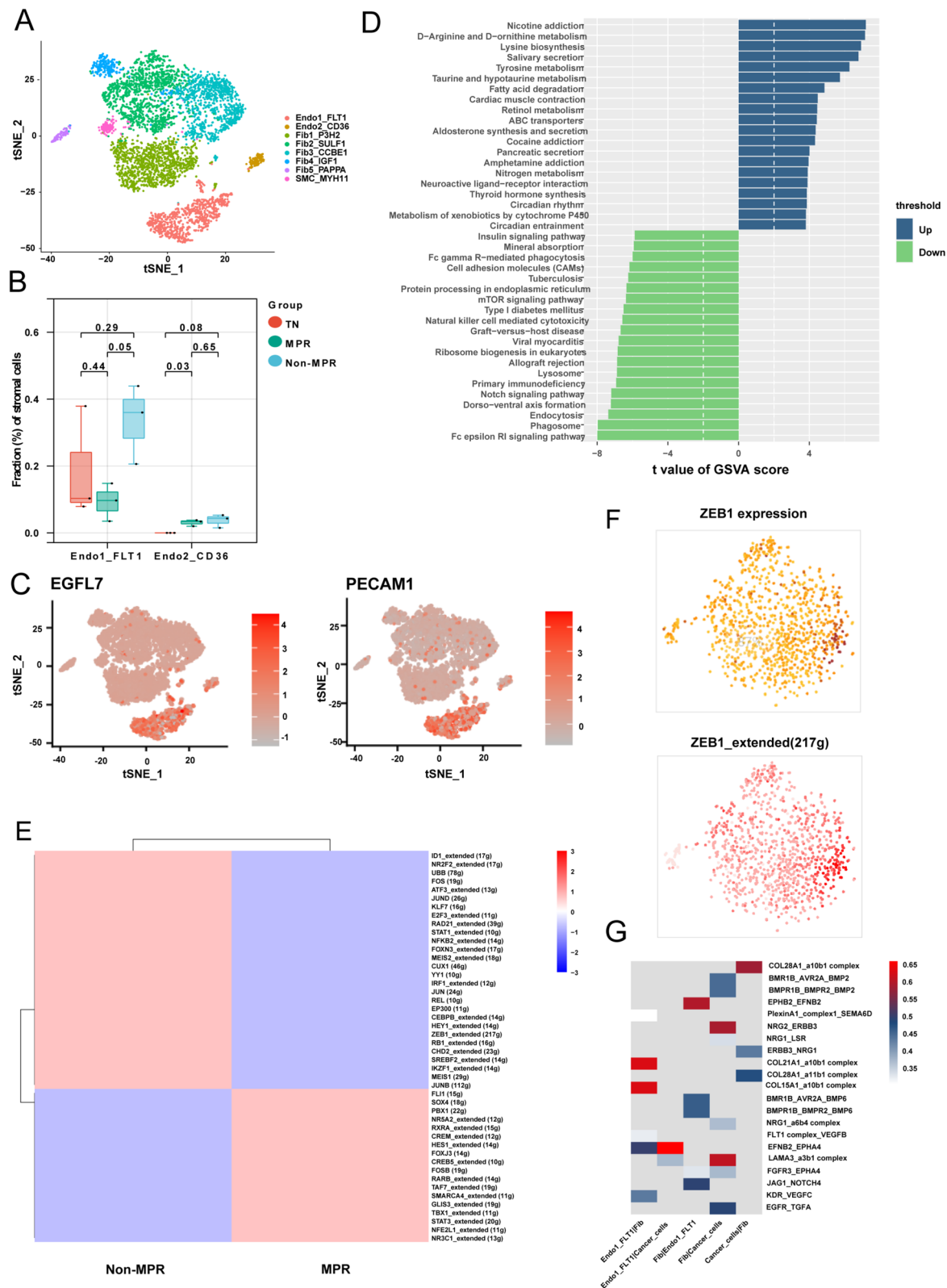
Recently, a review summarized the new progress of cancer immune evasion, enriched and expanded the "3E" model, and proposed a new "3C" conceptual framework. This immunoevasive phenotype arises from a variety of mechanisms and can be summarized as camouflage, coercion, and cytoprotection [22]. With a renewed appreciation of the immunoevasive capacity of tumor cells, we found that current single drug with PD-1 blockade is limited, and simultaneous blockade of multiple immunoevasive pathways is required to enhance immunotherapy and ultimately activate anticancer immune surveillance. Then, the choice of immune combination therapy strategy is crucial.

Vascular defects leading to some degree of hypoxia are common in most solid tumors and are accompanied by

(See figure on next page.)

**Fig. 5** Endothelial cells may regulate FLT1 response to anlotinib through ZEB1. **A** tSNE plot of stromal cells color-coded by clusters. **B** Box plot of fractions of Endo1\_FLT1 and Endo2\_CD36 cells in TN (n = 3), MPR (n = 3), and Non-MPR (n = 3) patients. The middle line represents the median, the lower and upper lines represent the 25th and 75th percentiles, respectively, with each point corresponding to one sample. t test was used for data analysis. **C** tSNE plot of normalized expression of Endo1\_FLT1 cells marker genes. **D** KEGG pathway comparison between MPR and Non-MPR endothelial cell by GSVA. **E** Heat map of the area under the curve (AUC) scores of expression regulation by transcription factors, as estimated using Single-cell regulatory network inference and clustering (SCENIC), for endothelial cells from Non-MPR and MPR. **F** tSNE plot of endothelial cells for the expression of ZEB1 (top) by SCENIC, and for (bottom) the AUC of the estimated regulon activity of ZEB1, corresponding to the degree of expression regulation of target genes. **G** Heat map of the interactions among fibroblasts, Endo1\_FLT1 cells and cancer cells





immunosuppression [23]. HIF-induced VEGFA secretion is a signal for the activation of "coercion" immunoevasive mechanism in "3C" model. Anti-angiogenic agents targeting VEGF-A/VEGFR can help limit tumor-induced immunosuppression. Based on interesting preclinical studies, many clinical trials have been conducted to investigate the efficacy of anti-VEGFA/VEGFR therapy combined with immune checkpoint blockade, thus approving these associations in different tumor sites [24].

During the last decade, different anti-angiogenic agents have been developed and approved to treat cancer patients. Anti-angiogenic therapy can be responsible for a transient normalization of the vasculature favoring tumor infiltration by immune cells. In this study, we found that the proportions of T cell subpopulations and myeloid cell subpopulations were different in TN, MPR and Non-MPR groups. These results once again demonstrate the remodeling effect of anlotinib on the immune microenvironment. On the other hand, it suggests that we should search for markers related to combination treatment response in the differences, which is also the work that clinical research must complete in the era of precision medicine. Therefore, we need to further analyze the evolution of tumor cells and speculate the potential resistance mechanism of Non-MPR group.

T cells cooperate with B cells to coordinate the cellular and humoral arms of adaptive immunity against pathogens or inflammatory diseases. Complex signaling events triggered by the multi-subunit T cell antigen receptor controlled the development, activation and differentiation of T cells into effector cells. Preliminary study had shown that deletion of *Themis* causes CD4<sup>+</sup> and CD8<sup>+</sup> T cells in mice fail to proliferate effectively and upregulate activated markers upon TCR stimulation [25]. Further analysis showed that *THEMIS* was required to promote optimal Treg suppressive function and that the prevalence of the disease could be reduced following transfer of wild-type Treg into the mutated rat lines [26]. Intra-tumoral infiltration of T<sub>THEMIS</sub> cells may suppress the tumor immune microenvironment, but the role of peripheral blood is still unknown. As potential predictor factors, further demonstration of its superiority in early screening is needed.

The main resistance mechanism of anti-angiogenic agents is the activation of alternative pro-angiogenic pathways such as angiopoietin-2 (Ang2)/Tie2, HGF/c-Met or PIGF [27, 28]. In patients with metastatic melanoma treated with ICB, high levels of Ang2 are associated with poor response to bevacizumab therapy [29]. However, we found differential expression of PLA2G4A in the treatment groups, a key enzyme in the VEGF pathway. PLA2G4A is a subunit of cytosolic PLA2 (cPLA2).

The products of PLA2G4A could modulate inflammatory responses pathways. Recent research reported that PLA2G4A regulate CD39<sup>+</sup>  $\gamma\delta$  Treg polarization to promote metastasis through the arachidonic acid metabolic pathway [30]. A variety kind of tumor cells can escape from immune surveillance by releasing bioactive lipids into immune microenvironment involved in metabolic coercion [31]. Bioactive lipids including PGE2 and lysoglycerophospholipids are produced by the membrane-released arachidonic acid [32]. Recently, several reports shown that PGE2 can promote immune escape by directly affecting the function and survival of tumor infiltrating CD8<sup>+</sup> CTLs, and PGE2 could favor immunosuppression during pancreatic tumorigenesis by driving the differentiation of tumor-infiltrating monocytes into M2-like TAMs [33, 34]. Therefore, PLA2 have been considered as potential therapeutic targets for many years [35]. However, most PLA2 inhibitors fail in clinical trials due to their poor efficacy and adverse effects, there are three main reasons for this failure: (i) redundancy between PLA2 isoforms, (ii) the lack of selective inhibitors, and (iii) a lack of knowledge of the roles of PLA2 isoforms in each type of cancer [36]. Optimizing compound design and functional lipidomics is essential for the development of selective inhibitors of PLA2 isoforms.

This study explored predictive factors and resistance mechanisms with limited sequencing results, and validation in public databases was insufficient. A complete experimental design that interprets the prominent role of specific cell populations in the remodeling of the tumor immune microenvironment,

(See figure on next page.)

**Fig. 6** cPLA2 promoted Tregs infiltration and drug resistance. **A** tSNE plot of epithelial cell color-coded by clusters. **B** Bubble plot for the enrichment analysis of differentially expressed genes between MPR and Non-MPR cancer cells by KEGG. **C** Box plot of fractions of epithelial cells in TN (n = 3), MPR (n = 3), and Non-MPR (n = 3) patients. The middle line represents the median, the lower and upper lines represent the 25th and 75th percentiles, respectively, with each point corresponding to one sample. t test was used for data analysis. **D** Immunohistochemistry (IHC) staining of FoxP3, CD4 and PLA2G4A in NSCLC cohort, representative photos are shown. **E** The association of FoxP3 and CD4 with PLA2G4A was analyzed. **F** Forest plot showing the independent prognostic factors for OS in NSCLC cohort (n = 135, multivariate Cox regression analysis). **G** Overall survival according to PLA2G4A expression level by Kaplan–Meier in NSCLC cohort

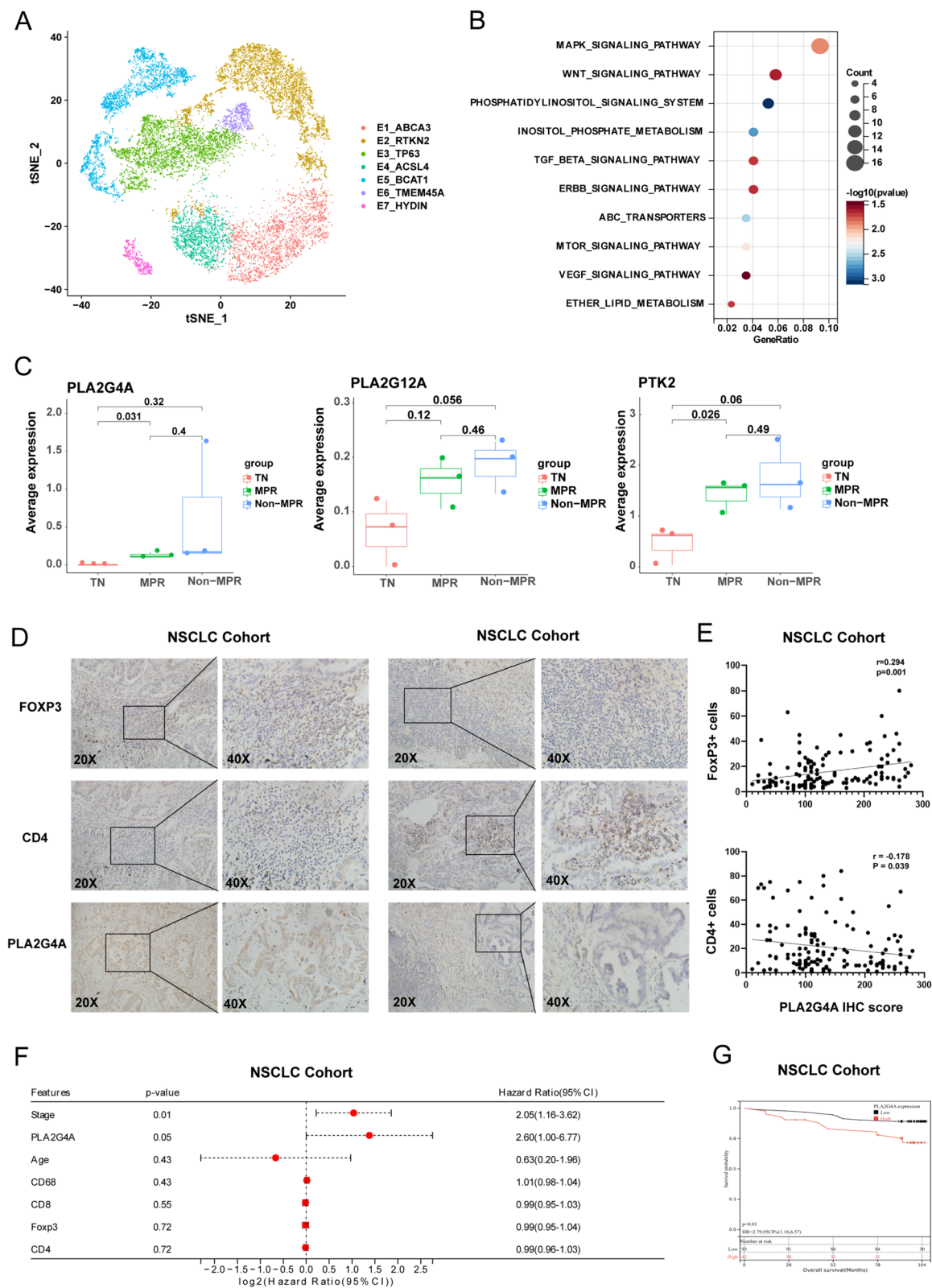


**Fig. 6** (See legend on previous page.)

and then blocking this effect will help to select patient populations and increase patients benefit.

## Conclusions

In this study, we constructed a comprehensive single-cell transcriptomic atlas of NSCLC patients received neoadjuvant anlotinib combined with PD-1 blockade therapy, revealed the cellular population heterogeneity in the tumor immune microenvironment and the possible underlying mechanism of failed treatment. We found that the dynamic changes of VEGF signaling dependent endothelial and epithelial cells have a profound impact on the formation of anlotinib resistance and immunosuppressive phenotypes in NSCLC patients.

## Abbreviations

NSCLC	Non-small cell lung cancer
MPR	Major pathological response
TAMs	Tumor-associated macrophages
VEGFA	Vascular endothelial growth factor A
VEGFR	Vascular endothelial growth factor receptor
CNVs	Copy number variations
mIHC	Multiplex immunofluorescence
Ang2	Angiopoietin-2
cPLA2	Cytosolic PLA2
VEGF	Vascular endothelial growth factor
tSNE	T-distributed stochastic neighbor embedding
AUC	Area under the curve
SCENIC	Single-cell regulatory network inference and clustering
IHC	Immunohistochemistry

## Supplementary Information

The online version contains supplementary material available at <https://doi.org/10.1186/s12967-025-06485-4>.

Additional file 1: Figure S1. Single-cell clusters and interaction network. (A) tSNE plot of all cells color-coded into 23 clusters. (B) tSNE plot of all cells color-coded from TN, MPR and Non-MPR patients. (C) Shell map of the interactions among SMC cells and other cell types. Figure S2. Marker genes of T cells and trajectory analysis. (A) tSNE plot of normalized expression of T cells marker genes among clusters. (B) Box plot of fractions of CD4<sup>+</sup> T and CD8<sup>+</sup> T cells in TN (n = 3), MPR (n = 3), and Non-MPR (n = 3) patients. The middle line represents the median, the lower and upper lines represent the 25th and 75th percentiles, respectively, with each point corresponding to one sample. t test was used for data analysis. (C) Box plots of the average exhausted signature scores for CD4<sub>CD28</sub>, CD4<sub>CD40LG</sub>, and NK<sub>KLRD1</sub> cells in TN (n = 3), MPR (n = 3), and Non-MPR (n = 3) patients. (D) The developmental trajectory of T cells inferred by Monocle2. The right cells were the roots of trajectory, and differentiated into left cells. (E) Heat map of the top50 differential genes in T<sub>THEMIS</sub> cells along the pseudo-time. Figure S3. Marker genes of B cells. (A) tSNE plot of marker genes of B cells among clusters. (B) tSNE plot of normalized expression of marker genes of B4<sub>PAX5</sub> memory B cells. Figure S4. Marker genes of myeloid cells and cell-interaction analysis. (A) tSNE plot of normalized expression of myeloid marker genes among clusters. (B) qPCR was used to detect the expression of DPP4 in A549 cells and CXCL2 and CCL3L3 in TAMs in the co-culture system treated with anlotinib (20 μM). (C) Heat map of the interactions between DC<sub>HDAC9</sub> and T<sub>THEMIS</sub> cells. Figure S5. Marker genes of stromal cells. (A) tSNE plot of normalized expression of marker genes of Endo1<sub>FLT1</sub>, Endo2<sub>CD36</sub>, Fib1<sub>P3H2</sub>, Fib2<sub>SULF1</sub>, Fib3<sub>CCBE1</sub>, Fib4<sub>IGF1</sub>, Fib5<sub>PAPPA</sub>, and SMC<sub>MYH11</sub> cells.

(B) qPCR was used to detect the expression of VEGFA and VEGFB in TAMs and VEGFR and ZEB1 in HUVEC in the co-culture system treated with anlotinib (20 μM). Figure S6. InferCNV analysis and fractions of epithelial cells. (A) Heat map of identification of malignant cells with myeloid cells as control group by inferCNV. (B) Box plot of fractions of epithelial cells in TN (n = 3), MPR (n = 3), and Non-MPR (n = 3) patients. The middle line represents the median, the lower and upper lines represent the 25th and 75th percentiles, respectively, with each point corresponding to one sample. t test was used for data analysis. (C) qPCR was used to detect the expression of PTK2, PLA2G4A and PLA2G12A in A549 cells in the co-culture system treated with anlotinib (20 μM). (D) Overall survival according to PLA2G4A expression level by Kaplan–Meier in TCGA database.

Additional file 2: Table S1. Clinical information of scRNA-seq samples. Table S2. Gene list of function modules. Table S3. Clinical information of IHC cohort. Table S4. Primer sequences.

## Acknowledgements

The authors would like to thank Peng Zhang and Chinese Academy of Science for their providing the single-cell sequencing data of TN samples.

## Author contributions

Z.H. and M.W. contributed to the conception and design of the study. B.L., M.S. and Q.W. are responsible for collecting and collating documents. L.L., H.J. and Q.Z. performed these experiments. Z.H., X.Z. and Y.Z. participated in analysis and interpretation of the data. Z.H., L.L. and L.Y. are responsible for writing this article. All authors contributed to the article and approved the submitted version.

## Funding

This work was supported by the National Natural Science Foundation of China (No. 82472983, No. 82103001, and No. 82403866), Natural Science Foundation of Tianjin (No. 22JCYBJC01050), China Anti-Cancer Association Foundation (No. 2021001012), Beijing Medical Public Welfare Foundation (No. YWJKJHKYJJ-LD-LC022), and Tianjin Municipal Science and Technology Program (No. 24KPMRC00140).

## Availability of data and materials

Requests for further information and resources should be directed to and will be fulfilled by the lead contact, Lili Yang (yanglili@tjmuch.com). The single-cell RNA-seq data can be accessed through NCBI GEO under Accession Number GSE291670.

## Declarations

### Ethics approval and consent to participate

The use of patient information and tissues was approved by the Ethics Committee of the Tianjin Medical University Cancer Institute and Hospital (Ek2022273). The patients provided their written informed consent to participate in this study.

### Consent for publication

Not applicable.

### Competing interests

The authors declare that they have no competing interests.

### Author details

<sup>1</sup>Department of Immunology, Tianjin's Clinical Research Center for Cancer, Key Laboratory of Cancer Immunology and Biotherapy, State Key Laboratory of Druggability Evaluation and Systematic Translational Medicine, Tianjin Medical University Cancer Institute and Hospital, National Clinical Research Center for Cancer, Huanhuxi Road, Tiyanbei, Hexi District, Tianjin 300060, China. <sup>2</sup>Department of Esophageal Cancer, Tianjin's Clinical Research Center for Cancer, Key Laboratory of Cancer Prevention and Therapy, Tianjin Medical University Cancer Institute and Hospital, National Clinical Research

Center for Cancer, Tianjin, China. <sup>3</sup>Department of Lung Cancer, Tianjin's Clinical Research Center for Cancer, Key Laboratory of Cancer Prevention and Therapy, Tianjin Medical University Cancer Institute and Hospital, National Clinical Research Center for Cancer, Huanhuxi Road, Tiyanbei, Hexi District, Tianjin 300060, China.

Received: 11 January 2025 Accepted: 11 April 2025

Published online: 25 April 2025

## References

- Desai AP, Adashek JJ, Reuss JE, West HJ, Mansfield AS. Perioperative immune checkpoint inhibition in early-stage non-small cell lung cancer: a review. *JAMA Oncol.* 2023;9(1):135–42.
- Forde PM, Spicer J, Lu S, Provencio M, Mitsudomi T, Awad MM, et al. Neoadjuvant nivolumab plus chemotherapy in resectable lung cancer. *N Engl J Med.* 2022;386(21):1973–85.
- Cascone T, William WN, Weissferdt A, Leung CH, Lin HY, Pataer A, et al. Neoadjuvant nivolumab or nivolumab plus ipilimumab in operable non-small cell lung cancer: the phase 2 randomized NEOSTAR trial. *Nat Med.* 2021;27(3):504–14.
- Schuler M, Cuppens K, Plönes T, Wiesweg M, Du Pont B, Hegedus B, et al. Neoadjuvant nivolumab with or without relatlimab in resectable non-small-cell lung cancer: a randomized phase 2 trial. *Nat Med.* 2024;30(6):1602–11.
- Xia H, Zhang H, Ruan Z, Zhang H, Sun L, Chen H, et al. Neoadjuvant camrelizumab (an anti-PD-1 antibody) plus chemotherapy or apatinib (a VEGFR-2 inhibitor) for initially unresectable stage II–III non-small-cell lung cancer: a multicentre, two-arm, phase 2 exploratory study. *Signal Transduct Target Ther.* 2024;9(1):145.
- Zhao J, Zhao L, Guo W, Wang S, Tao X, Li L, et al. Efficacy, safety, and biomarker analysis of neoadjuvant camrelizumab and apatinib in patients with resectable NSCLC: a phase 2 clinical trial. *J Thorac Oncol.* 2023;18(6):780–91.
- Ho QT, Kuo CJ. Vascular endothelial growth factor: biology and therapeutic applications. *Int J Biochem Cell Biol.* 2007;39(7–8):1349–57.
- Huang H, Langenkamp E, Georganaki M, Loskog A, Fuchs PF, Dieterich LC, et al. VEGF suppresses T-lymphocyte infiltration in the tumor microenvironment through inhibition of NF- $\kappa$ B-induced endothelial activation. *FASEB J.* 2015;29(1):227–38.
- Dikov MM, Ohm JE, Ray N, Tchekneva EE, Burlison J, Moghanaki D, et al. Differential roles of vascular endothelial growth factor receptors 1 and 2 in dendritic cell differentiation. *J Immunol.* 2005;174(1):215–22.
- Voron T, Colussi O, Marcheteau E, Pernot S, Nizard M, Pointet A-L, et al. VEGF-A modulates expression of inhibitory checkpoints on CD8<sup>+</sup> T cells in tumors. *J Exp Med.* 2015;212(2):139–48.
- Sun Y, Niu W, Du F, Du C, Li S, Wang J, et al. Safety, pharmacokinetics, and antitumor properties of anlotinib, an oral multi-target tyrosine kinase inhibitor, in patients with advanced refractory solid tumors. *J Hematol Oncol.* 2016;9(1):105.
- Zhang C, Chu T, Wang Q, Cheng Y, Zhang Y, Wang R, et al. Enhancement of anti-PD-L1 antibody plus anlotinib efficacy due to downregulation of PD-L1 in the micro-conduit endothelium within the tumor: a randomized double-blind trial. *Cancer Biol Med.* 2024.
- Liu S, Qin T, Liu Z, Wang J, Jia Y, Feng Y, et al. anlotinib alters tumor immune microenvironment by downregulating PD-L1 expression on vascular endothelial cells. *Cell Death Dis.* 2020;11(5):309.
- Luo J, Cheng K, Ji X, Gao C, Zhu R, Chen J, et al. Anlotinib enhanced CD8<sup>+</sup> T cell infiltration via induction of CCL5 improves the efficacy of PD-1/PD-L1 blockade therapy in lung cancer. *Cancer Lett.* 2024;591:216892.
- Tang H, You T, Ge H, Gao J, Wang Y, Bai C, et al. Anlotinib may enhance the efficacy of anti-PD1 therapy by inhibiting the AKT pathway and promoting the apoptosis of CAFs in lung adenocarcinoma. *Int Immunopharmacol.* 2024;133:112053.
- Yuan S, Peng L, Liu Y, Till BG, Yan X, Zhang J, et al. Low-dose anlotinib confers improved survival in combination with immune checkpoint inhibitor in advanced non-small cell lung cancer patients. *Cancer Immunol Immunother.* 2023;72(2):437–48.
- Yu L, Xu J, Qiao R, Zhong H, Brueckl WM, Zhong R. Comparative efficacy and safety of multitarget angiogenesis inhibitor combined with immune checkpoint inhibitor and nivolumab monotherapy as second-line or beyond for advanced lung adenocarcinoma in driver-negative patients: a retrospective comparative cohort study. *Transl Lung Cancer Res.* 2023;12(5):1108–21.
- Dou X-J, Ma R-Y, Ren D-W, Liu Q, Yan P. Effectiveness and safety of anlotinib combined with PD-1 blockades in patients with previously immunotherapy treated advanced non-small cell lung cancer: a retrospective exploratory study. *Lung Cancer (Auckl).* 2024;15:29–40.
- Gascoigne NRJ, Acuto O. THEMIS: a critical TCR signal regulator for ligand discrimination. *Curr Opin Immunol.* 2015;33:86–92.
- Chen L, Xie X, Wang T, Xu L, Zhai Z, Wu H, et al. ARL13B promotes angiogenesis and glioma growth by activating VEGFA-VEGFR2 signaling. *Neuro Oncol.* 2023;25(5):871–85.
- Murakami M, Kudo I. Phospholipase A2. *J Biochem.* 2002;131(3):285–92.
- Galassi C, Chan TA, Vitale I, Galluzzi L. The hallmarks of cancer immune evasion. *Cancer Cell.* 2024;42:1825.
- Hanahan D. Hallmarks of cancer: new dimensions. *Cancer Discov.* 2022;12(1):31–46.
- Bourhis M, Palle J, Galy-Fauroux I, Terme M. Direct and indirect modulation of T cells by VEGF-A counteracted by anti-angiogenic treatment. *Front Immunol.* 2021;12:616837.
- Fu G, Vallée S, Rybak V, McGuire MV, Ampudia J, Brockmeyer C, et al. Themis controls thymocyte selection through regulation of T cell antigen receptor-mediated signaling. *Nat Immunol.* 2009;10(8):848–56.
- Chabod M, Pedros C, Lamouroux L, Colacios C, Bernard I, Lagrange D, et al. A spontaneous mutation of the rat Themis gene leads to impaired function of regulatory T cells linked to inflammatory bowel disease. *PLoS Genet.* 2012;8(1):e1002461.
- Kopetz S, Hoff PM, Morris JS, Wolff RA, Eng C, Glover KY, et al. Phase II trial of infusional fluorouracil, irinotecan, and bevacizumab for metastatic colorectal cancer: efficacy and circulating angiogenic biomarkers associated with therapeutic resistance. *J Clin Oncol.* 2010;28(3):453–9.
- Itatani Y, Kawada K, Yamamoto T, Sakai Y. Resistance to anti-angiogenic therapy in cancer-alterations to anti-VEGF pathway. *Int J Mol Sci.* 2018;19(4).
- Goede V, Coutelle O, Neuneier J, Reinacher-Schick A, Schnell R, Koslowsky TC, et al. Identification of serum angiopoietin-2 as a biomarker for clinical outcome of colorectal cancer patients treated with bevacizumab-containing therapy. *Br J Cancer.* 2010;103(9):1407–14.
- Zhan Y, Zheng L, Liu J, Hu D, Wang J, Liu K, et al. PLA2G4A promotes right-sided colorectal cancer progression by inducing CD39<sup>+</sup> $\gamma$  $\delta$  Treg polarization. *JCI Insight.* 2021;6(16).
- Bayerl F, Meiser P, Donakonda S, Hirschberger A, Lacher SB, Pedde A-M, et al. Tumor-derived prostaglandin E2 programs cDC1 dysfunction to impair intratumoral orchestration of anti-cancer T cell responses. *Immunity.* 2023;56(6):1341.
- De Martino M, Rathmell JC, Galluzzi L, Vanpouille-Box C. Cancer cell metabolism and antitumor immunity. *Nat Rev Immunol.* 2024;24(9):654–69.
- Lacher SB, Dörr J, de Almeida GP, Hönninger J, Bayerl F, Hirschberger A, et al. PGE2 limits effector expansion of tumour-infiltrating stem-like CD8<sup>+</sup> T cells. *Nature.* 2024;629(8011):417–25.
- Caronni N, La Terza F, Vittoria FM, Barbiera G, Mezzananza L, Cuzzola V, et al. IL-1 $\beta$  macrophages fuel pathogenic inflammation in pancreatic cancer. *Nature.* 2023;623(7986):415–22.
- Nikolaou A, Kokotou MG, Vasilakaki S, Kokotos G. Small-molecule inhibitors as potential therapeutics and as tools to understand the role of phospholipases A2. *Biochim Biophys Acta Mol Cell Biol Lipids.* 2019;1864(6):941–56.
- Peng Z, Chang Y, Fan J, Ji W, Su C. Phospholipase A2 superfamily in cancer. *Cancer Lett.* 2021;497:165–77.

## Publisher's Note

Springer Nature remains neutral with regard to jurisdictional claims in published maps and institutional affiliations.